First principle energies of binary and ternary phases of the Fe–Nb–Ni–Cr system

Damien Connetable, Muriel Mathon, Jacques Lacaze

▶ **To cite this version:**

Damien Connetable, Muriel Mathon, Jacques Lacaze. First principle energies of binary and ternary phases of the Fe–Nb–Ni–Cr system. Calphad, 2011, 35 (4), pp.588-593. 10.1016/j.calphad.2011.09.004 . hal-00701527

HAL Id: hal-00701527
https://inria.hal.science/hal-00701527

Submitted on 25 Jan 2022

HAL is a multi-disciplinary open access archive for the deposit and dissemination of scientific research documents, whether they are published or not. The documents may come from teaching and research institutions in France or abroad, or from public or private research centers.

L'archive ouverte pluridisciplinaire **HAL**, est destinée au dépôt et à la diffusion de documents scientifiques de niveau recherche, publiés ou non, émanant des établissements d'enseignement et de recherche français ou étrangers, des laboratoires publics ou privés.

Open Archive Toulouse Archive Ouverte (OATAO)
OATAO is an open access repository that collects the work of Toulouse researchers and makes it freely available over the web where possible.

This is an author-deposited version published in: http://oatao.univ-toulouse.fr/
Eprints ID: 5546

To link to this article: DOI: 10.1016/j.calphad.2011.09.004
URLhttp://dx.doi.org/10.1016/j.calphad.2011.09.004

To cite this version:

Connétable, Damien and Mathon, Muriel and Lacaze, Jacques *First principle energies of binary and ternary phases of the Fe–Nb–Ni–Cr system.* (2011) Calphad, vol. 35 (n° 4). pp. 588-593. ISSN 0364-5916

Any correspondence concerning this service should be sent to the repository administrator: staff-oatao@listes.diff.inp-toulouse.fr

First principle energies of binary and ternary phases of the Fe–Nb–Ni–Cr system

Damien Connétable *, Muriel Mathon, Jacques Lacaze

CIRIMAT UMR 5085, CNRS-INP-UPS, École Nationale d'Ingénieurs en Arts Chimiques et Technologiques (ENSIACET) 4, allée Émile Monso, BP 44362, F-31030 Toulouse Cedex 4, France

A B S T R A C T

We present first principles enthalpies of formation and lattice parameters of iron, nickel, chromium and niobium alloys. Some of these results have been partially used in a recent assessment of the Fe–Ni–Cr–Nb quaternary phase diagram. Emphasis has been put on the fcc (A1) and bcc (A2) unary structures, the X_3Y-$D0_{22}$, -$L1_2$, -$D0_3$, -$D0_a$, X_2Y-C14($MgZn_2$), -C15($MgCu_2$) and -C36 ($MgNi_2$) Laves and X_7Y_6-$D8_5$ (μ) binary phases, and the $X_8Y_4Z_{18}$-$D8_b$ (σ) ternary phase. We employed the state of the art to compute their properties by means of the DFT (PBE functional and PAW pseudo potentials). A comparison with experimental and theoretical data is also provided.

Keywords:
First principles calculations
Formation energies
Nickel
Iron
Chromium
Niobium

1. Introduction

Inconel 718 is a nickel-based superalloy used in the aeronautic and nuclear industries. This material contains mainly Ni, Fe, Cr and a few atomic percent of Nb, Mo and Al, as well as smaller amounts of Ti, Co, C, Si, Mn and Ta. Its production involves thermo-mechanical and heat treatments that induce phase changes and give it its microstructure with high mechanical performance. The present work was carried out within a long-term study aiming at modeling the phase transformations during thermo-mechanical processing of Inconel 718. The phases that can appear during solidification and processing of this alloy are mainly fcc (γ) Ni-rich solid solution, $D0_a$-Ni_3Nb (δ), $D0_{22}$-Ni_3Nb (γ''), $L1_2$ (γ' or Ni_3Al), possibly MC and M_6C carbides, Laves and bcc (α) or hcp-Ni_3Ti (η).

The results presented below were used to generate a database for nickel superalloys. As a first step to build this thermodynamic database the quaternary system Ni–Nb–Fe–Cr was considered in which a large number of crystal structures (unary: X, binary: X/Y and ternary X/Y/Z) are required.

In modern Ni-based superalloys for airfoil turbines, the main hardening phase is represented by the $L1_2$ γ'-Ni_3Al phase, which was not studied here as it is not the predominant hardening phase for Nb-rich alloys like the alloys 706 and 718. In these latter alloys, the principal hardening mechanism is associated with the phase Ni_3Nb-$D0_{22}$. It is a metastable phase that transforms to the stable orthorhombic Ni_3Nb-$D0_a$ upon ageing. The precipitation of the metastable $D0_{22}$ phase is achieved by heat-treating the Nb-supersaturated gamma phase at a temperature between 1023 and 873 K [1–4].

In superalloys, the Laves phases have a negative impact on the mechanical properties, because they precipitate at grain boundaries and are factors of embrittlement. The presence of Laves phase Fe_2Nb formed after ageing for various times at 1048 K has been noted by Peard and Borland [5] in a 56.4% Fe–3.8% Nb–39.8% Ni alloy. Savin [6] also studied ternary alloys of Fe–Nb–Ni, quenched from the liquid state. At the highest rates, amorphous materials and phases such as C15 or distorted $D8_5$ appear. They noted a C36 formation for the composition 40% Fe–40% Ni–20% Nb. Peard and Borland [5] also noted the presence of orthorhombic $D0_a$ (Fe, Ni)Nb in the alloy 56.4% Fe–3.8% Nb–39.8% Ni. In the Fe–Nb–Ni system, Ueyama et al. [7] have identified a $D0_a$ in a 10% Fe–15% Nb–75% Ni alloy equilibrated for 240 h at 1473 K and then water quenched.

The σ phase occurs in a number of binary and ternary systems involving transition-group elements [1]. It is brittle and is of technological importance in connection with stainless steels. The interest in the σ phase goes far beyond its technological properties and is related to the fundamental problem of structural stability in crystal chemistry and the physics of metals and alloys.

In this paper we present the results (lattice parameters and formation energies) of an *ab initio* study of Ni–Nb–Fe–Cr alloys. Emphasis was put on two unary structures, fcc (A1) and bcc (A2), eight binary phases, X_3Y-$D0_{22}$, -$L1_2$, -$D0_a$, -$D0_3$, $D8_5$ (Fe_7W_6-type, μ), X_2Y-C14 ($MgZn_2$), -C15 ($MgCu_2$) and -C36 ($MgNi_2$) Laves, and on the σ ternary phase (FeCr-type). In this work we compare

* Corresponding author.
E-mail address: damien.connetable@ensiacet.fr (D. Connétable).

doi:10.1016/j.calphad.2011.09.004

our results to experimental and theoretical information whenever available.

2. Computational details

The calculations were made within the density functional theory formalism (DFT) and the pseudo-potential approximation. They were performed by means of plane wave methods as implemented in the Vienna *ab initio* simulation program (VASP) [8]. We used Projected augmented waves pseudo potentials (PAW) [9], and the Perdew–Burke–Ernzerhof [10] generalized gradient approximation of the exchange and correlation functional. The pseudopotentials of Fe, Cr and Nb contain semi-core states, whereas those for Ni do not. Collinear magnetism (ferro and non magnetic structures) was taken into account in our simulations. The cut-off was fixed to 400 eV with Monkhorst Pack dense mesh grids (about 5000 **k** points atom/cell) to optimize the ground states, and to compute the converged formation energies we increased the convergence criteria to about 13 000 **k**-points atom/cell (equivalent by band-folding to a 24 × 24 × 24 **k**-grid for the reference states) with a higher energy cut-off (500 eV). For all structures, the **k**-mesh grids were not shifted (24 × 24 × 24 for cubic, hexagonal and orthorhombic structures). The Γ point is always included. The precision of the formation energies was in the range of about 1 meV/atom or 0.5 kJ/mol.

3. Results and discussion

3.1. Pure elements

Before studying the relative stability of binary and ternary phases, we firstly studied the fcc (A1) and bcc (A2) structures. These structures correspond to the reference states for Nb, Cr, Fe (bcc) and Ni (fcc). The results for the cohesive and formation energies for the unaries are defined as

$$E_c[X] = E_0^{bulk}[X] - E_X^{at} \quad (1)$$

and

$$E_f[X] = E_0^{bulk}[X] - E_0^{ref}[X] \quad (2)$$

where $E_0^{bulk}[X]$ is the reference energy of an X atom, E_X^{at} is the energy of an isolated X atom, and $E_0^{ref}[X]$ is the energy of the reference state are presented in Table 1. For these reference states, DFT simulations reproduce fairly well the experimental cohesive energies. In the case of fcc-Fe and bcc-Ni, the ground states are ferromagnetic, whereas fcc-Cr and Nb are found to be paramagnetic. Anti-ferromagnetism was not taken into account in our simulations. Moreover, we also report the results for Fe, Cr and Nb fcc and Ni bcc.

3.2. X_3Y–$L1_2$

The prototype of the cubic structure $L1_2$ is Cu_3Au (cP4, $Pm3m$, space group 221), where the atoms (4 per unit cell) are on the sites of a fcc lattice: the X atoms are in 3c (center of the face of the cube) and the Y atoms are located in 1a (see Fig. 1). To compute the formation energies of the binaries we defined E_f as

$$E_f[X_nY_m] = (E_0[X_nY_m] - nE_0^{ref}[X] - mE_0^{ref}[Y])/(n+m) \quad (3)$$

where E_0^{ref} are the energies of the reference states and $E_0[X_nY_m]$ is the energy of the system. The energies of the pure elements in the $L1_2$-fcc ordered phase are equal to the fcc A1 ones ($X_3X = A1$).

As one can see from Table 2, the formation energies of the Ni_3Y phases (where Y = Cr, Nb and Fe) are negative (underlined in Table 2), suggesting that these structures are thermodynamically

Table 1
Optimized lattice parameters (in Å), formation energies E_f (in meV/atom), cohesive energies E_c (in eV), and total magnetic moments (in Bohr's magneton, μ_b) of pure bcc and fcc phases.

System	a_o (Å)	E_f	E_c	μ	
bcc structures					
Nb*	3.313	–	7.06	0.0	
	3.30	–	7.57	0.0	Exp. [11]
Ni	2.805	929	–	0.54	
Fe*	2.839	–	5.07	2.24	
	2.87	–	4.28	2.20	Exp. [11]
Cr*	2.844	–	4.04	0.0	
	2.88	-	4.10	antiferro	Exp. [11]
fcc structures					
Nb	4.217	323	–	0.0	
Ni*	3.520	–	4.88	0.62	
	3.52	–	4.44	0.61	Exp. [11]
Fe	3.453	156	–	0.89	
Cr	3.625	388	–	0.0	

* Reference states.

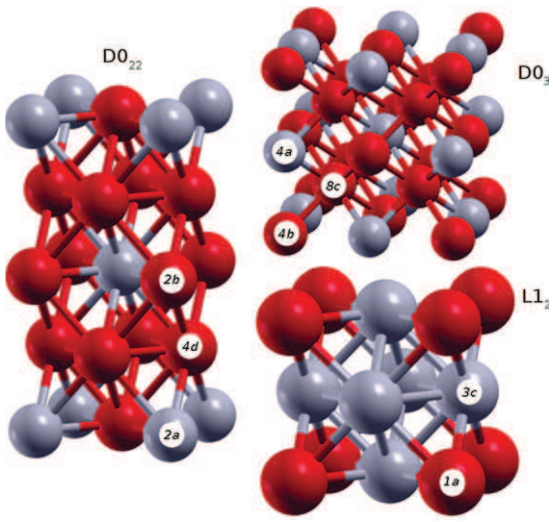

Fig. 1. Schematic representation of the $D0_{22}$, $D0_3$ and $L1_2$ structures.

favoured. Experimentally, the ordered Ni_3Fe-$L1_2$ is stable in the Fe–Ni phase diagram below 790 K. The optimized lattice parameters are in agreement with experimental data [12] and the calculated E_f values of Ni_3Fe and Ni_3Cr agree with previous calculated data [13].

3.3. X_3Y-$D0_{22}$ and -$D0_3$ structures

X_3Y-$D0_{22}$ and -$D0_3$ have tetragonal and cubic structures, respectively.

The first one, $D0_{22}$ (4 atoms per unit cell), is based on $TiAl_3$ (tI8, $I4/mmm$, space group 139), where the Al atoms are located in 4d, 2b, and Ti in 2a. The second one, $D0_3$ (4 atoms per unit cell), has a cubic structure (WFe_3 prototype, cF16, $Fm3m$, space group 225), where the Y atoms are in 4a, and the X atoms are in 4b and 8c (see Fig. 1). The atoms sit on the sites of a body centered cubic lattice.

There are many structures related to $D0_{22}$ and the continuity between different lattices depends on the tetragonal c/a ratio. Thus, when $c = 2a$, the atoms are on the sites of an fcc lattice, and when $a/c = \sqrt{2}$, $D0_{22}$ becomes $D0_3$. These relations have induced some difficulties in the optimization of unit cells, and many minima (absolute and local) are often noticed, depending on the values of the lattice parameters. The *ab initio* results, presented in the assessment published earlier [27], correspond to those of $D0_3$and not $D0_{22}$. For the present paper, $D0_{22}$ was computed again

Table 2
Optimized lattice parameters (in Å), formation energies E_f^1 (in meV/atom), E_f^2 (in kJ/mol), and total magnetic moments (in Bohr's magneton μ_b) of X_3Y-$L1_2$. We have underlined systems with negative energies.

X/Y	a_o (Å)	E_f^1	E_f^2	μ	
Nb/Ni	4.038	93	36.0	0.0	
Nb/Fe	4.038	313	120.9	0.0	
Nb/Cr	4.120	525	202.9	2.71	
Ni/Nb	3.689	−154	−59.3	0.81	
	3.640				Theo. [14]
Ni/Fe	3.548	−91	−35.2	4.78	
	3.545	−89			Theo. [13]
	3.52				Exp. [12]
Ni/Cr	3.565	−10	−3.7	2.17	
	3.55				Exp. [12]
Fe/Nb	3.715	17	6.6	3.58	
Fe/Ni	3.602	40	15.6	8.29	
	3.578	48			Theo. [13]
Fe/Cr	3.545	43	16.6	2.79	
Cr/Nb	3.801	486	187.4	1.9	
Cr/Ni	3.577	214	82.7	0.0	
Cr/Fe	3.575	243	93.9	0.21	

Table 3
Optimized lattice parameters (in Å), formation energies E_f^1 (in meV/atom), E_f^2 (in kJ/mol), and total magnetic moments (in Bohr's magneton μ_b) of $D0_3$ and $D0_{22}$. We have underlined systems with negative energies.

X/Y	a_o	c_o	E_f^1	E_f^2	μ	
X_3Y-$D0_{22}$						
Nb/Nb	3.879	9.812	144	55.6	0.0	
Nb/Ni	3.943	8.488	83	32.2	0.0	
Nb/Fe	3.772	9.174	210	81.3	0.0	
Nb/Cr	3.768	9.486	256	98.7	0.0	
Ni/Nb	3.643	7.484	−308	−118.7	0.0	
	3.63	7.42	–	–	–	Exp. [15]
Ni/Ni	3.520	7.058	0	0.0	2.5	
Ni/Fe	3.546	7.104	−76	−29.2	4.5	
Ni/Cr	3.490	7.194	4	1.4	0.0	
Fe/Nb	3.569	8.258	14	5.5	5.7	
Fe/Ni	3.472	7.378	84	32.3	2.3	
Fe/Fe	3.462	6.884	161	62.1	0.0	
Fe/Cr	3.480	7.026	120	46.4	0.0	
Cr/Nb	3.494	8.888	334	129.1	0.0	
Cr/Ni	3.580	7.138	178	68.7	0.0	
Cr/Fe	3.537	7.338	256	99.0	0.0	
Cr/Cr	2.793	7.076	274	105.7	0.0	
X_3Y-$D0_3$						
Nb/Ni	6.416		21	8.0	0.0	
Nb/Fe	6.355		7	2.7	0.1	
Nb/Cr	6.412		81	31.3	0.0	
Ni/Nb	5.862		−145	−55.7	0.0	
Ni/Fe	5.650		17	6.4	4.4	
Ni/Cr	5.653		107	41.4	2.0	
Fe/Nb	5.898		−69	−26.5	5.1	
Fe/Ni	5.690		292	111.8	3.0	
Fe/Cr	5.669		60	23.2	5.6	
Cr/Nb	5.952		68	26.2	0.0	
Cr/Ni	5.700		218	84.2	0.1	
Cr/Fe	5.697		116	44.6	2.0	

and new formation energies and lattice parameters are reported. Results for $D0_3$and $D0_{22}$ are listed in Table 3. Only two $D0_{22}$ (Ni_3Y where Y = Nb or Fe) structures are found to be thermodynamically favored, and one $D0_3$ (Ni_3Nb). These results are in agreement with experimental observations.

Due to the importance of the metastable Ni_3Nb-$D0_{22}$ phase, its elastic constants were computed [16]. The elastic constants of fcc-Ni, bcc-Nb and Ni_3Nb-$D0_{22}$ are reported in Table 4. Our results are in agreement with experimental data [11,17] for reference states and with previous calculations of $D0_{22}$ [18]. The elastic behavior of Ni_3Nb is found to be close to that of nickel. From these data, we computed the bulk and shear moduli (within the Reuss, Voigt and Hill approximations) (B_o and $G_{H,R,V}$), the Young's modulus (E), and the Poisson's ratio (ν), following relations given previously in [19]. The anisotropy was also investigated. The bulk modulus along the *a*, *b* and *c* axes (see appendix of [20]), and the shear anisotropic factors (A_i, a measure of the degree of elastic anisotropy) were computed. The results are reported in Table 5.

Table 4
Comparison of the elastic constants (in GPa) of the Ni_3Nb-$D0_{22}$, Nb-bcc and Ni-fcc phases.

	C_{11}	C_{12}	C_{13}	C_{33}	C_{44}	C_{66}	B_o
Ni-fcc	274	160	–	–	130	–	198
	250[a]	150[a]	–	–	131[a]	–	198[b]
Ni_3Nb-$D0_{22}$	285	180	159	306	113	119	208
	288[c]	188[c]	162[c]	299[c]	115[c]	104[c]	211[c]
Nb-bcc	235	137	–	–	16	–	170
	236[a]	139[a]	–	–	29[a]	–	173[b]

[a] Exp. [17].
[b] Exp. [11].
[c] Theo. [18].

Table 5
Reuss, Voigt and Hillt ($B_{H,R,V}$, in GPa) bulk modulus, bulk modulus along *x*, *y* and *z* directions ($B_{a,b,c}$, in GPa), anisotropic parameters ($A_{1,2,3}$), Young's modulus (E, in GPa), Poisson's ratio (ν) and shear modulus (G, in GPa).

	$B_{H,R,V}$	$B_{a,b}$	B_c	$G_{R,V}$	G_H
Ni	198	594	594	101	93
Ni_3Nb-$D0_{22}$	208	624	624	94	90
Theo.[18]	211	656	591	91	86
Nb	171	513	513	29	25
	$A_{1,2}$	A_3	E	ν	
Ni	2.28	2.28	242	0.30	
Ni_3Nb-$D0_{22}$	1.66	2.27	235	0.31	
Theo. [18]	1.75	2.08	228	0.32	
Nb	0.33	0.33	72	0.43	

Plotting the directional bulk modulus B_o showed that B_o is isotropic (spherical shape), in spite of tetragonal symmetry of the system. This is confirmed by the values of B_a, B_b and B_c which are all equal.

3.4. X_2Y-C36, -C14 and -C15 Laves phases

We have studied the three polymorphs of the Laves phase of composition X_2Y: C36, C15 and C14. C36 (24 atoms/uc) is a hexagonal structure (see Fig. 2), with $MgNi_2$ as prototype (hP24, $P6_3/mmc$, No. 194). Y atoms are located in 4e, 4f, and X in 6g, 6h and *4f*. C14 (12 atoms/uc) has also a hexagonal symmetry, $MgZn_2$-prototype (hP12, $P6_/mmc$, space group 194), with Y atoms located in 4f and X in 2a, 6h. Finally, C15 (6 atoms/uc), is based on $MgCu_2$, it is a cubic structure (cF24, $Fd3m$, space group 227) where the Y atoms are in 8a and the *X* atoms are in 16d sites of the diamond like structure.

The results are listed in Tables 6–8. The Cr–Nb binary has been studied experimentally and theoretically by Grujicic et al. [21] and Pavlů et al. [22], respectively. In this system Cr_2Nb is present at high temperature as C14 and as C15 at low temperature. Moreover, C14 is also observed in the Fe–Nb phase diagram as Fe_2Nb. We find that X_2Nb (where X = Ni, Fe and Cr)-C14, -C15 and -C36 have negative energies. In the previous study [27], one mistake appeared for Cr_2Nb-C14, which is corrected here. A discussion of the magnetic properties of Fe_2Nb-C14 was presented previously [27]. We can note that C14 is found to be weakly ferromagnetic, in agreement with our simulations (1.6 μ_b). Our results are in agreement with experimental data for Cr_2Nb, though C36 could have been expected in the phase of C14. While Ni_2Nb appears to be highly favored, it does not show up in the Ni–Nb system where Ni_3Nb appears instead.

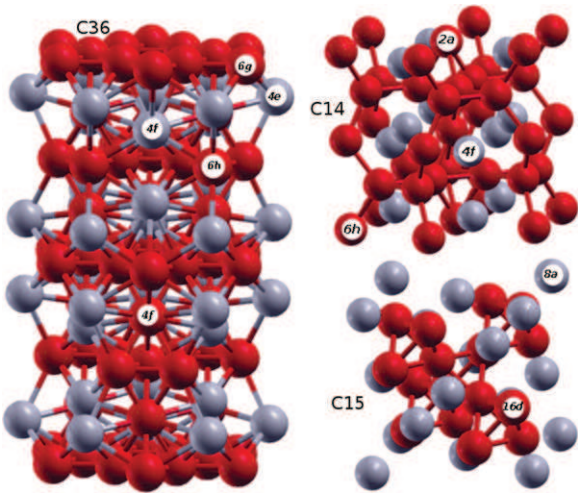

Fig. 2. Schematic representation of the X_2Y-C14, -C15 and -C36 Laves.

Table 6
Optimized lattice parameters (in Å), formation energies E_f^1 (in meV/atom), E_f^2 (in kJ/mol), and total magnetic moments (in Bohr's magneton μ_b) of X_2Y-C36. We have underlined systems with negative energies.

X/Y	a_o	c_o	E_f	E_c	μ	
Nb/Nb	5.460	17.585	315	729.4	0.0	
	5.48	17.52				Theo. [22]
Nb/Ni	5.273	17.027	540	1249.8	0.0	
Nb/Fe	5.248	16.904	783	1813.3	0.0	
Nb/Cr	5.339	17.224	693	1604.9	11.2	
	5.32	17.15				Theo. [22]
Ni/Nb	4.805	15.648	−194	−449.8	2.3	
Ni/Ni	4.615	14.948	215	498.0	13.8	
Ni/Fe	4.637	15.098	89	207.3	32.6	
Ni/Cr	4.587	15.037	240	556.3	0.3	
Fe/Nb	4.793	15.822	−158	−366.6	8.1	
Fe/Ni	4.645	15.124	184	425.8	39.2	
Fe/Fe	4.555	14.845	367	849.6	8.8	
Fe/Cr	4.665	15.184	153	354.9	6.6	
Cr/Nb	4.911	16.060	−44	−101.7	0.0	
	4.90	16.02				Theo. [22]
	4.82	15.77	−58		–	Theo. [23]
	4.87	15.26				Exp. [21]
Cr/Ni	4.658	15.097	274	635.5	0.0	
Cr/Fe	4.627	14.985	309	716.2		
Cr/Cr	4.681	15.310	281	649.9	0.4	
	4.65	15.23				Theo. [22]

When a Laves phase is stable in a binary system, it is seen that the other two Laves phases have very similar E_f. This is in line with the well known fact that various forms of Laves phases appear in either binary or ternary systems when varying the temperature and composition, as it is the case for the Cr–Nb system. In most cases, unstable Laves phases show similar positive E_f values for each X/Y combination. There are, however, a few exceptions: C14–Nb_2Fe and –Fe_2Fe that have less positive values than the two other forms, while C36-Fe_2Fe shows much higher values than the other variants (the magnetism is not able to explain this "anomaly").

To complete the description of the stable structures, we report, for information, in Table 9 optimized internal parameters. From one composition to another, these parameters vary only slightly (less than 5%).

3.5. X_7Y_6-$D8_5$

The prototype of $D8_5$ is Fe_7W_6 (labeled μ) with 13 atoms per unit cell. X_7Y_6-$D8_5$ has a trigonal structure (hR13, *R*3*m*, space group 166), where the *X* atoms are in 1a and 6h, and the *Y* atoms are in $2c^3$ (see Fig. 3). $D8_5$ is present in the Ni–Nb and Fe–Nb systems.

Table 10 shows that X_7Nb_6 (where X = Ni and Fe) and Cr_7Y_6 (where Y = Ni and Nb) have negative formation energies. Read et al. [25] studied the magnetic properties of the $D8_5$ phase in Fe–Nb, and he concluded that $D8_5$ is anti-ferromagnetic below 270 K. In our simulations, restricting us to ferromagnetic behaviors, we found that Fe_7Nb_6 is ferromagnetic, with a total magnetic moment equal to about 8.6 μ_b. The difference in energy is generally small. For other structures, no experimental values have been reported.

3.6. X_3Y-$D0_a$

$D0_a$ is based on the orthorhombic Cu_3Ti-prototype (oP8, *Pmmn*, space group 59). The *X* atoms are in 2b, 4f and the Y atoms are

Table 7
Optimized lattice parameters (in Å), formation energies E_f (in meV/atom and kJ/mol), and total magnetic moments (in Bohr's magneton) of X_2Y-C14. We have underlined systems with negative energies.

X/Y	a_o	c_o	E_f^1	E_f^2	μ	
Nb/Nb	2.746	8.642	162	187.2	0.0	
	2.75	8.68				Theo. [22]
Nb/Ni	2.648	8.381	555	642.4	0.0	
Nb/Fe	2.624	8.198	21	24.8	0.0	
Nb/Cr	2.741	8.033	743	860.8	0.0	
	2.69	8.36				Theo. [22]
Ni/Nb	2.405	7.808	−201	−232.3	0.0	
Ni/Ni	2.312	7.440	201	233.0	7.1	
Ni/Fe	2.324	7.502	83	96.2	16.4	
Ni/Cr	2.350	6.622	184	213.2	15.9	
Fe/Nb	2.384	7.875	−150	−174.1	1.6	
Fe/Ni	2.319	7.540	189	218.4	19.1	
Fe/Fe	2.345	7.668	152	175.8	29.2	
Fe/Cr	2.325	7.470	174	201.8	2.9	
Cr/Nb	2.450	8.083	−35	−40.0	0.0	
	2.42	8.06				Theo. [22]
	2.42	7.87				Theo. [23]
	2.47	8.07				Exp. [24]
Cr/Ni	2.338	7.534	288	333.6	0.0	
Cr/Fe	2.317	7.459	322	372.8	0.0	
Cr/Cr	2.335	7.691	290	335.3	−0.3	
	2.32	7.66				Theo. [22]

Table 8
Optimized lattice parameters (in Å), formation energies E_f (in meV/atom and kJ/mol), and total magnetic moments (in Bohr's magneton) of X_2Y-C15. We have underlined systems with negative energies.

X/Y	a_o	E_f^1	E_f^2	μ	
Nb/Nb	7.678	163	94.2	0.0	
	7.69				Theo. [22]
Nb/Ni	7.429	511	295.8	0.0	
Nb/Fe	7.393	780	451.6	0.0	
Nb/Cr	7.456	626	362.2	5.7	
	7.50				Theo. [22]
Ni/Nb	6.795	−188	−108.8	2.0	
Ni/Ni	6.527	227	131.4	3.4	
Ni/Fe	6.562	99	57.6	8.1	
Ni/Cr	6.483	259	150.1	0.0	
Fe/Nb	6.799	−148	−86.0	4.8	
Fe/Ni	6.563	178	102.8	9.9	
Fe/Fe	6.444	359	207.8	6.7	
Fe/Cr	6.440	263	152.6	0.0	
Cr/Nb	6.949	−48	−27.6	0.0	
	6.93				Theo. [22]
	6.82				Theo. [23]
	6.991	−77			Exp. [24]
Cr/Ni	6.574	261	150.8	0.0	
Cr/Fe	6.521	297	172.0	0.0	
Cr/Cr	6.616	276	160.0	0.0	
	6.58				Theo. [22]

Table 9
Internal parameters of stable structures (C14, C36, $D8_5$ and $D0_a$).

C36-X_2Nb	X	4*f*	1/3	2/3	0.1236
	X	6g	1/2	0	0
	X	6h	0.1639	0.3278	1/4
	Nb	4e	0	0	0.0946
	Nb	4f	1/3	2/3	0.8435
C14-X_2Nb	X	2a	0	0	0
	X	6h	0.8311	0.6622	1/4
	Nb	4f	1/3	2/3	0.0553
$D8_5$-X_7Nb_6	X	1a	0	0	0
	X	6h	0.0907	0.5904	0.0907
	Nb	2c	0.1683	0.1683	0.1683
	Nb	2c	0.3445	0.3445	0.3445
	Nb	2c	0.4510	0.4510	0.4510
$D0_a$-X_3Y	Y	2b	1/2	1/2	0.3479
	Y	4f	0.2493	0	0.1601
	X	2a	0	0	0.6520

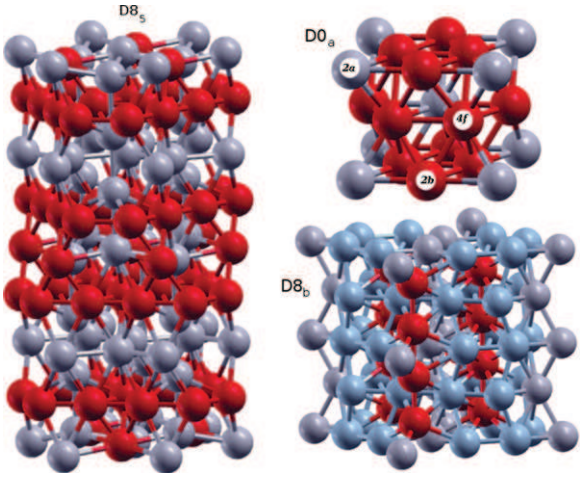

Fig. 3. Schematic representation of the $D8_5$, $D0_a$ and σ-$D8_b$ structures.

Table 10
Optimized lattice parameters (in Å), formation energies E_f^1 (in meV/atom) E_f^2 (in kJ/mol), and total magnetic moments (in Bohr's magneton μ_b) of X_7Y_6-$D8_5$. We have underlined systems with negative energies.

X/Y	a_o	c_o	E_f^1	E_f^2	μ
Nb/Nb	5.433	9.515	167	209.3	0.0
Nb/Ni	5.265	8.628	349	437.2	0.0
Nb/Fe	5.252	8.608	705	883.8	0.0
Nb/Cr	5.301	8.739	685	859.4	0.4
Ni/Nb	4.879	8.789	−223	−280.2	0.1
Ni/Ni	4.613	8.040	164	206.2	7.7
Ni/Fe	4.631	8.174	30	37.4	29.9
Ni/Cr	4.586	8.136	157	196.8	2.1
Fe/Nb	4.870	8.880	−140	−175.7	8.6
Fe/Ni	4.620	8.145	117	146.8	18.8
Fe/Fe	4.568	8.043	235	294.6	10.1
Fe/Cr	4.584	8.144	114	143.3	3.6
Cr/Nb	4.920	9.212	−8	−10.0	0.2
Cr/Ni	4.610	8.233	−136	−170.2	0.0
Cr/Fe	4.604	8.323	194	243.0	9.8
Cr/Cr	4.639	8.422	221	277.7	2.8

in 2a (see Fig. 3). Ni_3Nb (δ) is the only known $D0_a$ phase in the Fe–Ni–Nb–Cr quaternary system.

The results are listed in Table 11. *Ab initio* simulations reproduce the experimental data on Ni_3Nb fairly well. We also predict another

Table 11
Optimized lattice parameters (in Å), formation energies E_f^1 (in meV/atom), E_f^2 (in kJ/mol), and total magnetic moments (in Bohr's magneton μ_b) of X_6Y_2-$D0_a$. We have underlined systems with negative energies.

X/Y	a_o	b_o	c_o	E_f^1	E_f^2	μ	
Nb/Nb	5.318	4.999	5.580	194	150.0	0.0	
Nb/Ni	6.391	4.521	4.519	20	15.6	0.0	
Nb/Fe	6.345	4.489	4.486	7	5.7	0.0	
Nb/Cr	5.196	4.662	5.562	294	226.8	0.0	
Ni/Nb	5.117	4.254	4.551	−314	−242.6	0.0	
	5.073	4.194	4.505			0.0	Theo. [14]
	5.122	4.234	4.505	–		0.0	Exp. [26]
Ni/Ni	4.980	4.086	4.315	24	18.5	5.1	
Ni/Fe	5.026	4.069	4.366	−76	−59.0	9.2	
Ni/Cr	5.648	3.999	3.999	108	83.1	4.2	
Fe/Nb	5.063	4.163	4.751	49	37.8	5.1	
Fe/Ni	5.738	4.041	4.040	28	21.4	17.3	
Fe/Fe	4.908	3.884	4.253	84	65.1	0.0	
Fe/Cr	4.963	3.953	4.308	68	52.4	0.0	
Cr/Nb	5.952	4.212	4.217	69	52.5	0.0	
Cr/Ni	5.039	4.034	4.536	187	144.8	0.0	
Cr/Fe	4.855	4.028	4.710	264	204.3	0.0	
Cr/Cr	4.601	4.237	4.863	315	243.1	0.0	

Table 12
Optimized lattice parameters (in Å), formation energies E_f^1 (in meV/atom), E_f^2 (in kJ/mol), and total magnetic moments (in Bohr's magneton μ_b) of $X_8Y_4Z_{18}$-σ. We have underlined systems with negative energies.

X/Y/Z	a_o	c_o	E_f^1	E_f^2	μ
Ni/Nb/Nb	9.715	5.257	209	605.8	0.0
Ni/Nb/Ni	8.763	4.625	−72	−207.7	0.1
Ni/Nb/Fe	8.820	4.692	8	24.5	39.9
Ni/Nb/Cr	8.850	4.770	132	383.1	0.0
Ni/Cr/Nb	9.570	5.160	226	654.5	0.0
Fe/Nb/Nb	8.849	5.198	254	734.0	15.8
Fe/Nb/Ni	8.839	4.644	−65	−185.6	24.8
Fe/Nb/Fe	8.926	4.692	−0	−0.3	54.7
Fe/Nb/Cr	8.778	4.787	153	444.3	12.0
Fe/Cr/Nb	9.691	5.095	304	880.9	19.5
Fe/Fe/Cr	8.649	4.617	143	415.3	17.6
Fe/Cr/Fe	8.448	4.462	171	494.7	15.0
Fe/Cr/Cr	8.650	4.630	131	378.2	12.1
Cr/Cr/Fe	8.645	4.495	63	181.3	20.2
Cr/Fe/Cr	8.768	4.577	155	448.4	8.5
Cr/Fe/Fe	8.626	4.460	98	285.2	12.1

favored structure, Ni_3Fe, which is not present in the Ni–Fe phase diagram.

3.7. $X_8Y_4Z_{18}$-σ

Due to the complex structure of σ phase ($X_8Y_4Z_{18}$), we have restricted ourself to some of them. $X_8Y_4Z_{18}$ is based on FeCr-σ ($D8_b$, $P4_2/mmm$, space group 136). σ is composed of five non equivalent positions, but only three sub-lattices were considered for the calculations. The *X* atoms are located in 8i, the Y atoms are in 4f and the Z atoms are in 2a, 8i and 8j, see Fig. 3. The first sub-lattice has been studied with Ni and Fe. The results are summarized in Table 12. Two systems ($X_8Nb_4Ni_{18}$, X = Ni and Fe) have negative energies.

3.8. Conclusion

In conclusion, we have presented a systematic *ab initio* study of the formation energies and lattice parameters of the unary and binary phases and one ternary phase of the Ni–Nb–Cr–Fe system. We reproduce satisfactorily the experimental values for the lattice parameters and formation energies, and propose

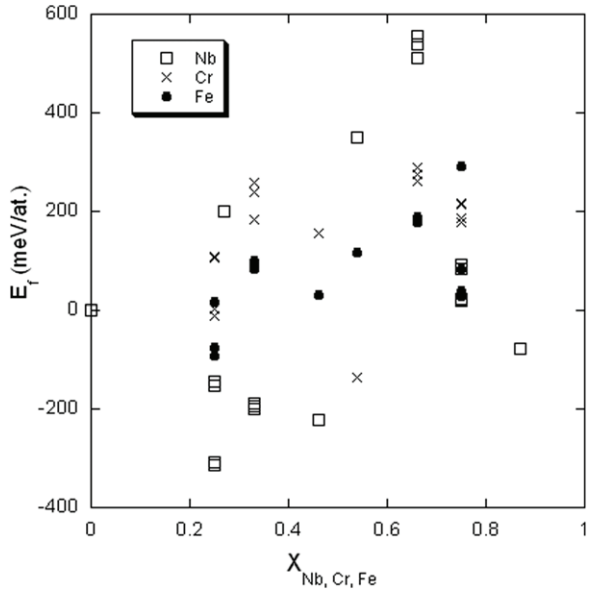

Fig. 4. Formation energies for the $Ni_{1-x}Y_x$ alloys as a function of the Y content expressed by x. Pentagons stand for Nb, stars for Cr and triangles for Fe.

formation energies for many metastable structures. In Fig. 4, we have summarized main results for the Ni–Y (Y = Fe, Nb and Cr) binary phases, for which many negative formation energies were found. Thus, this first-principles database should provide a good complement to the available CALPHAD thermodynamic databases.

Acknowledgments

The authors acknowledge the Midi-Pyrénées region for its financial support (No. 07009816). This work was granted access to the HPC resources of CALMIP (CICT Toulouse, France) under the allocation 2011-p0842.

References

[1] W.E. Quist, R. Taggart, D.H. Polonis, Metall. Trans. 2 (1971) 825–832.
[2] J. Manenc, J. Bourgeot, H. De Boer, Scr. Metall. 2 (1968) 453–458.
[3] I. Kirman, Scr. Metall. 2 (1968) 679–680.
[4] J. Manenc, Scr. Metall. 2 (1968) 705–706.
[5] K.A. Peard, D.W. Borland, Scr. Metall. 3 (1969) 267.
[6] V.V. Savin, Fiz. Met. Metalloved. 68 (1989) 143–149.
[7] T. Ueyama, M.M. Ghanem, N. Miura, M. Takeyama, T. Matsuo, Thermec'97, International Conference on Thermomechanical Processing of Steels and Others Materials, The Minerals, Metals and Materials Society, 1997, pp. 1753–1760.
[8] G. Kresse, J. Hafner, Phys. Rev. B 47 (1993) 558; 49 (1994) 14251; G. Kresse, J. Furthmüler, Phys. Rev. B 54 (1996) 11169; G. Kresse, J. Furthmüller, Comput. Mater. Sci. 6 (1996) 15.
[9] G. Kresse, D. Joubert, Phys. Rev. B 59 (1999) 1758.
[10] J.P. Perdew, K. Burke, M. Ernzerhof, Phys. Rev. Lett. 77 (1996) 3865; J.P. Perdew, K. Burke, M. Ernzerhof, Phys. Rev. Lett. 78 (1997) 1396.
[11] C. Kittel, Introduction to Solid State Physics, Wiley, New York, 1996.
[12] Y. Tanaka, S. Ishida, S. Asano, Mater. Trans. 46 (2005) 355.
[13] Y. Mishin, M.J. Mehl, D.A. Papaconstantopoulos, Acta Mater. 53 (2005) 4029.
[14] P. Ravindran, G. Subramoniam, R. Asokamani, Phys. Rev. B 53 (1995) 1129.
[15] Superalloys: a technical guide By Matthew J. Donachie, Stephen James Donachie ASM International, 2002 - Technology & Engineering.
[16] We employed six types of infinitesimal deformations to calculate C_{ij}. Curves were fitted with polynomial functions. $20 \times 20 \times 20$ k-grid and 500 eV energy cut-off were used as convergence criteria.
[17] G. Simmons, H. Wang, Single Crystal Elastic Constants and Calculated Aggregate Properties: A Handbook, second ed. MIT Press, Cambridge, MA, 1971.
[18] S. Dai, W. Liu, Comput. Mater. Sci. 49 (2010) 414–418.
[19] D. Connétable, O. Thomas, Phys. Rev. B 79 (2009) 094101.
[20] P. Ravindran, L. Fast, P.A. Korzhavyi, B. Johansson, J. Wills, O. Eriksson, J. Appl. Phys. 84 (1998) 4891.
[21] M. Grujicic, S. Tangrila, O.B. Cavin, W.D. Porter, C.R. Hubbard, Mater. Sci. Eng. A160 (1993) 37.
[22] J. Pavlü, J. Vřešťál, M. Šob, Calphad Comput. Coupling Phase Diagr. Thermochem. 33 (2009) 179.
[23] S. Hong, C.L. Fu, Intermetallics 7 (1999) 5.
[24] D.J. Thoma, J.H. Perezko, Mater. Sci. Eng. 1 156 (1992) 97.
[25] D.A. Read, G.C. Hallam, M.S. Sabota, A. Mustaffa, Phys. B 86–88 (1977) 66.
[26] T. Fang, S.J. Kennedy, L. Quan, T.J. Hicks, J. Phys.: Condens. Matter. 4 (1992) 2405.
[27] M. Mathon, D. Connétable, B. Sundman, J. Lacaze, Calphad Comput. Coupling Phase Diagr. Thermochem. 33 (2009) 136–161.